Sea ice switch mechanism and glacial-interglacial CO_2 variations

Hezi Gildor and Eli Tziperman

Environmental Sciences, Weizmann Institute, Rehovot, Israel

J. R. Toggweiler

Geophysical Fluid Dynamics Laboratory, Princeton, New Jersey, USA

[1]   A physical mechanism is proposed for the glacial-interglacial variations in the rate of vertical mixing and in sea ice cover in the Southern Ocean. Such variations were postulated without an explanation by *Toggweiler* [1999] and *Stephens and Keeling* [2000], who used them to explain the glacial-interglacial CO_2 variations. In the physical mechanism explored here, initially given by *Gildor and Tziperman* [2001b], changes in the stratification of the Southern Ocean due to the cooling of North Atlantic Deep Water (NADW) during glacial maxima reduce the rate of vertical mixing of the surface water with the deep water. The changed temperature of the NADW arriving to the Southern Ocean and the reduced vertical mixing there also increase the Southern Ocean sea ice cover during glacial maxima. These vertical mixing and sea ice cover changes are shown to be a natural result of the sea ice switch mechanism of the glacial cycles. A box model of the climate system is used to demonstrate the above physical mechanism and its effect on the atmospheric CO_2. Because of the uncertainties in the exact dependence of the vertical mixing on vertical stratification, it is impossible to quantify the exact separate contribution of reduced vertical mixing and larger sea ice cover to the glacial CO_2 variations. The CO_2 variations are not essential to the existence of the glacial cycles in the sea ice switch mechanism, yet they are shown to amplify the glacial-interglacial variability, consistent with the view of the role of CO_2 deduced from proxy observations.   *INDEX TERMS:* 4806 Oceanography: Biological and Chemical: Carbon cycling; 4540 Oceanography: Physical: Ice mechanics and air/sea/ice exchange processes; 3344 Meteorology and Atmospheric Dynamics: Paleoclimatology

1.   Introduction

[2]   The atmospheric concentration of CO_2 has undergone significant and fairly regular variations on a timescale of 100 kyr during at least the last four glacial-interglacial cycles [*Petit et al.*, 1999], with concentrations during glacial periods being $\sim$80 ppm less than during warmer interglacial periods. Despite the effort invested in order to identify the mechanism responsible for these variations in light of the possible role it may play in global warming, a generally accepted explanation is still missing [*Pedersen and Bertrand*, 2000; *Sigman and Boyle*, 2000]. Previous explanations of this CO_2 variability in terms of Southern Ocean productivity and vertical mixing changes [*Wenk and Siegenthaler*, 1985; *Sarmiento and Toggweiler*, 1984; *Volk and Hoffert*, 1985] ran into contradicting evidence from various proxy indicators [*Toggweiler*, 1999]. The search for a mechanism, though, still seems focused on the Southern Ocean as the key region [*Pedersen and Bertrand*, 2000], although not exclusively [e.g., *Daskal Hausman and McElroy*, 1999]. *Stephens and Keeling* [2000] suggested that an extended sea ice cover during glacial

periods reduced air-sea CO_2 gas exchange. The extended sea ice cover was specified in their model based on available proxy records, but they didn't suggest a mechanism that can explain the extended sea ice cover. *Francois et al.* [1997] found evidence in the proxy record for an increased stratification southward of the polar front, which may have reduced the CO_2 leak from the ocean to atmosphere. Similarly, *Toggweiler* [1999] used a biochemical box model to suggest that by considering the Southern Ocean to be an upwelling region rather than a downwelling region, as done in previous works, a change in the vertical mixing in the Southern Ocean can induce the observed atmospheric CO_2 changes and still remain consistent with available proxy observations. *Toggweiler* [1999], again, did not propose a physical mechanism for a reduced vertical mixing in the Southern Ocean during glacial times.

[3]   *Stephens and Keeling* [2000] and *Toggweiler* [1999] presented restricted glacial and interglacial steady state solutions to their biochemical box models but could not explain the transition between these states. Dealing with the transition mechanism and explaining the changes in vertical mixing and sea ice cover clearly requires a physical mechanism and model of the glacial-interglacial cycle that is sufficiently detailed.

[4] Such a physical mechanism and model for the 100-kyr glacial oscillations was presented by *Gildor and Tziperman* [2000, 2001a, 2001b], including simplified yet explicit model components for the oceanic meridional circulation, sea ice, land glaciers, and atmosphere. This "sea ice switch" mechanism is based on a rapid switch-like growth and melting of the Northern Hemisphere sea ice. The sea ice, in turn, shifts the land ice between growing and withdrawing modes, creating the observed sawtooth structure and 100-kyr timescale. *Gildor and Tziperman* [2001b] have added an ocean biochemistry model to the physical climate model of *Gildor and Tziperman* [2000, 2001a] and have presented a detailed mechanism for the vertical mixing and sea ice changes arbitrarily specified by *Toggweiler* [1999] and *Stephens and Keeling* [2000]. The result is a possible scenario for the glacial oscillations, including the reduction of atmospheric CO$_2$ concentration during glacial periods, and the physical and biogeochemical mechanisms involved in both the glacial and interglacial stages, as well as the transitions between them.

[5] The mechanism suggested by *Gildor and Tziperman* [2001b] for the missing physics in the biochemical scenarios of *Toggweiler* [1999] and *Stephens and Keeling* [2000] may be summarized as follows. During the present interglacial period the stratification in the Southern Ocean is composed of cold fresh upper water above salty and warmer North Atlantic Deep Water (NADW) arriving to the Southern Ocean from the north. Note that this deeper water mass is relatively warm, also, due to mixing with surface midlatitude water on its way from the North Atlantic. We propose that during the buildup stage of Northern Hemisphere ice sheets the deep water formed in the North Atlantic becomes colder. Similarly, the mixing with cooler glacial period surface water in midlatitudes results in the subsurface deeper water arriving colder and denser to the Southern Ocean. This is in agreement with proxy records that indicate colder deep water in the Atlantic Ocean during the Last Glacial Maximum (LGM) [*Schrag et al.*, 1996] and with model results that show that NADW formation continues somewhat reduced during the LGM [*Ganopolski et al.*, 1998; *Weaver et al.*, 1998; *Yu et al.*, 1996; *Matsumoto and Lynch-Stieglitz*, 1999] and that the outflow to the Southern Ocean then becomes colder [*Weaver et al.*, 1998]. Because of the large ice mass over Antarctica, the surface water in the Southern Ocean is already very close to the freezing point, even during interglacial times, and cannot cool further during glacial maxima. The cooling of the deep water arriving from the North Atlantic therefore makes the stratification in the Southern Ocean more stable during glacial maxima, consistent with the proxy records of *Francois et al.* [1997]. On the basis of simple arguments linking the stratification to vertical mixing by internal waves [*Gargett*, 1984], such a more stable stratification is expected to reduce the mixing between the CO$_2$-rich deep water and the surface water [*Sikes et al.*, 2000]. This results in the observed reduction in atmospheric CO$_2$ during glacial periods, according to the mechanism of *Toggweiler* [1999]. The temperature, the vertical mixing, and the amount of the upwelling water also play key roles in controlling the Southern Ocean's sea ice [*Gordon*, 1981]: The reduced vertical mixing and the lower deep water

temperature result in a larger sea ice extension during cold periods [*Crosta et al.*, 1998]. This, in turn, can again reduce atmospheric CO$_2$ according to the mechanism of *Stephens and Keeling* [2000], who specified the sea ice change without providing a mechanism.

[6] In this proposed mechanism the glacial oscillations exist due to a self-sustained internal variability of the physical climate system, with Milankovitch forcing providing the phase locking of the 100-kyr variability [*Gildor and Tziperman*, 2000]. The CO$_2$ changes are therefore not the driving force of the glacial-interglacial oscillation [*Loutre and Berger*, 2000] but rather are induced by the physical changes to the Southern Ocean stratification and vertical mixing. These CO$_2$ changes, in turn, also affect the atmospheric radiation, and amplify the physical signal of the glacial oscillations to some degree, consistent with other model results [*Weaver et al.*, 1998] and with the recent interpretation of the Vostok record [*Petit et al.*, 1999].

[7] In the present paper we extend the work of *Gildor and Tziperman* [2001b], having in mind several specific objectives. First, we try to separate the contribution of changes in the rate of vertical mixing and in the sea ice cover to the glacial-interglacial CO$_2$ variations. Second, in light of the debate that arose recently in the literature regarding the differences between box models and general circulation model (GCM) simulations of the carbon cycle [*Archer et al.*, 2000b, 2000a; *Broecker et al.*, 1999], we try to test the sensitivity of the proposed mechanism to various processes that may contribute to these differences. (This issue is investigated more fully by J. Toggweiler et al. (Representation of the carbon cycle in box models and GCMs, 1, The solubility pump, and Representation of the carbon cycle in box models and GCMs, 2, The organic carbon pump, submitted to *Global Biogeochemical Cycles*, hereinafter referred to as T01a and T01b (available at http://www.ldeo.columbia.edu/~hezi/misc.html)) who demonstrated that with respect to organically cycled CO$_2$, box models may actually do a better job in simulating the partitioning of CO$_2$ between the ocean and the atmosphere.) Finally, we describe here the models used at a level of detail not possible in the short format of *Gildor and Tziperman* [2001b]. We start with a brief description of the physical model and its variation from a similar one used by *Gildor and Tziperman* [2000, 2001a] (section 2.1), describe the added biochemistry model (section 2.2), and explain the sea ice switch mechanism of glacial oscillations (section 3). Next, we combine the sea ice switch mechanism with the ocean biochemistry model and obtain the glacial atmospheric CO$_2$ variability based on the mechanism of *Toggweiler* [1999] (section 3.2). The sensitivity to the insulating effect of sea ice cover on the air-sea CO$_2$ flux [*Stephens and Keeling*, 2000], to the vertical mixing, to the piston velocity, and to the deep horizontal mixing are examined in sections 4.1, 4.2, 4.3, and 4.4, respectively. We conclude in section 5.

2. Model Description

2.1. Submodels for Physical Climate Component

[8] Our coupled meridional box model, schematically shown in Figure 1, is composed of ocean, atmosphere, sea
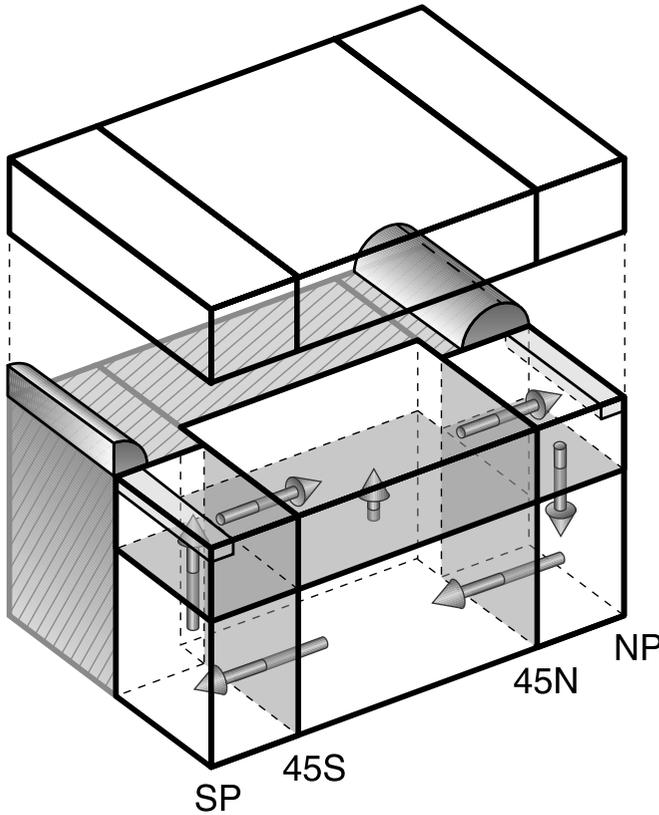
Figure 1. Schematic representation of coupled box model used in this study, showing atmospheric boxes (upper slab), thermohaline circulation (arrows), parabolic land ice sheets over land, and a partial sea ice cover in the polar ocean boxes. All of these physical climate system components are allowed to vary based on model equations. Ocean biogeochemistry and atmospheric CO$_2$ fully interact with physical climate components. See color version of this figure at back of this issue.

ice, and land ice models, including an active ocean biogeochemistry and a variable atmospheric CO$_2$, which may change due to exchanges with the ocean. The coupled ocean, atmosphere, sea ice, and land ice model is very similar to the one used and described in detail by *Gildor and Tziperman* [2000], *Gildor and Tziperman* [2001a]. We therefore describe the model briefly, emphasizing the changes made for the present study. Table 1 describes the model parameters whose values are different from those of *Gildor and Tziperman* [2001a]. The ocean is represented in

our model by three surface boxes and three deep boxes and represents both hemispheres. The polar boxes represent the regions between 45° and the poles, while the midlatitude box includes the regions between 45°S and 45°N. The meridional thermohaline circulation (THC) through the northern box is governed by the standard balance between horizontal friction and meridional pressure gradient [*Stommel*, 1961]. It is known that the THC dynamics in the Southern Ocean are different from those of the Northern Hemisphere. The upwelling of water in the south is the result of the westerly winds there, driving a northward Ekman drift and thus driving an upwelling in the Southern Ocean [*Toggweiler and Samuels*, 1993; *Gnanadesikan*, 1999]. Because the exact dependence of the upwelling on the intensity of the wind and on sea ice cover is still unclear, we have chosen to fix the intensity of the upwelling (and thus of the THC) through the southern polar box to a specified value (16 Sv). As the THC through the southern box is taken to be constant, the variability of the THC through the northern boxes affects only the amplitude of the THC that upwells in the midlatitude box. The ocean temperature and salinity are driven by air-sea fluxes of heat and fresh water, as well as by fresh water fluxes from land ice ablation and runoff. In the present version of the model the vertical mixing parameterization between the southern surface and deep boxes follows *Gargett* [1984], who proposed that the vertical mixing coefficient should be of the form $K_v = K_0 \left(\frac{\partial \rho}{\partial z}\right)^{-\alpha}$. In our box model, therefore, the vertical mixing term of any tracer T_r (e.g., temperature, salinity, or ΣCO_2) is a function of the vertical stratification,

$$K_v^0 \left(\sigma_{t_{\text{deep}}} - \sigma_{t_{\text{surface}}}\right)^{-\alpha} \left(T_{r_{\text{deep}}} - T_{r_{\text{surface}}}\right), \qquad (1)$$

where $\alpha = 1$. Upper and lower bounds on the instantaneous mixing rates $K_v^0 \left(\sigma_{t_{\text{deep}}} - \sigma_{t_{\text{surface}}}\right)^{-\alpha}$ of 280 and 1 Sv are also imposed. The vertical mixing coefficient between the other surface and deep boxes is constant, with a vertical mixing rate of 0.5 and 5 Sv between the midlatitude and the northern surface and deep boxes, respectively (the sensitivity to this constant is examined in section 4.2). The horizontal mixing scheme is also different from that of *Gildor and Tziperman* [2000a]. The model differentiates between horizontal mixing in the deep ocean (with mixing coefficient $K_{h_{\text{deep}}}$) and horizontal mixing between the surface boxes (with mixing coefficient $K_{h_{\text{up}}}$). The mixing coefficient in the deep ocean that is needed to produce the glacial-interglacial cycle in atmospheric CO$_2$ in our model seems somewhat too large, but it still represents an improvement relative to most box models,

Table 1. Parameters That Have Changed From *Gildor and Tziperman* [2001a]

Parameter, Unit	Description	Previous Value	New Value
r, s^{-1}	friction coefficient	$3. \times 10^{-4}$	2.2×10^{-4}
$K_{h_{\text{deep}}}$, m s^{-1}	deep horizontal mixing coefficient	3.5×10^{-4}	7.5×10^{-3}
$K_{h_{\text{up}}}$, m s^{-1}	surface horizontal mixing coefficient	3.5×10^{-4}	0.6×10^{-3}
K_v^0	vertical mixing		0.7×10^{-7}
τ, s	restoring time for Haney type heat flux	8.7×10^{-7}	4.65×10^7
$P_{1w1},..., P_{1w4}$	atmospheric emissivity	0.58, 0.56, 0.54, 0.626	0.61,0.49,0.52,0.67
$D_{sea\ ice}$, m	sea ice thickness	2	south 1.5, north 3

Table 2. Biochemistry Model Parameters

Parameter, Unit	Description	Value
r_1, r_2, r_3, mW	productivity coefficient	$6 \times 10^{-7}, 5. \times 10^{-4}, 1. \times 10^{-4}$
PV, m s^{-1}	piston velocity	$5. \times 10^{-5}$
TC_0	initial averaged total CO_2	2240, μmol, Kg^{-1}
TA_0	initial averaged total alkalinity	2371, μequiv, Kg^{-1}
P_0	initial averaged phosphate	2.09, μmol, Kg^{-1}

which treat the whole deep ocean as a single-value box [*Toggweiler*, 1999; *Stephens and Keeling*, 2000; *Volk and Hoffert*, 1985; *Wenk and Siegenthaler*, 1985; *Daskal Hausman and McElroy*, 1999].

[9] Sea ice forms in our model when the ocean water temperature decreases below a critical freezing temperature and melts above that temperature. Following the observed characteristic of sea ice in both hemispheres, the sea ice cover is assumed to grow in area within the northern and southern polar ocean boxes with an initial thickness of 3 and 1.5 m, respectively, and then to become thicker if the entire polar box is sea ice covered; sea ice presence and evolution affect the surface albedo, the salinity budget in the ocean, the air-sea heat flux, the CO_2 flux, and evaporation by partially insulating the ocean from the atmosphere. The equation of state is the full nonlinear equation recommended by *U.N. Educational, Scientific, and Cultural Organization* [1981].

[10] The atmospheric model is also similar to that used by *Gildor and Tziperman* [2001a], with a few changes. In order to improve the seasonality of sea ice cover, mainly in our southern box, we incorporate the important contribution of short-wave radiation to sea ice thermodynamics. The short-wave radiation term that influences the energy balance of sea ice can be written as [*Maykut and Perovich*, 1987]

$$(1 - \alpha)(1 - i_0)H_{in},$$

where α is the sea ice albedo and i_0 is the fraction of the net short-wave radiation that affects the atmospheric head balance and does not contribute directly to surface melting. Although both α and i_0 in reality are highly dependent on variables such as the type of sea ice, its age, etc., here we take them to be constants with the values of 0.65 and 0.57, respectively, giving together $(1 - \alpha)(1 - i_0) = 0.15$, i.e, 15%. The present model uses 15% of the incoming short-wave radiation, H_{in}, for melting of sea ice if and where it exists. The rest of the short-wave radiation directly influences the atmospheric heat balance, as before.

[11] The lower surface of each atmospheric box is a combination of ocean, land, land ice, and sea ice, each with its specified albedo. The averaged potential temperature of each atmospheric box is calculated based on the energy balance of the box.

[12] The outgoing long-wave radiation in the ith box is $H_{out} = P_{lw}^i \sigma \theta^4$, where σ is the Stefan-Boltzmann constant and P_{lw}^i is an emissivity coefficient that, in principal, depends on cloud cover, aerosol, etc. and is therefore allowed to vary here from box to box. In the present study, unlike in the work by *Gildor and Tziperman* [2000, 2001a], atmospheric CO_2 is a prognostic variable that directly

affects the long-wave emissivity,

$$P_{lw}^i = P_{lw,0}^i - K \log \frac{CO2}{CO_2^{ref}}, \quad (2)$$

where $P_{lw,0}^i$ is taken to be constant in time, CO_2 is the atmospheric concentration of carbon dioxide, CO_2^{ref} is a reference concentration taken to be 200 ppm, and K is chosen such that doubling the CO_2 concentration will cause a radiative forcing of 4 W m^{-2} [*Ramanathan et al.*, 1987].

[13] The model for northern land ice sheets, whose slow evolution provides the 100-kyr timescale in our model, is zonally symmetric, assumes perfect plasticity [*Weertman*, 1976; *Ghil*, 1994], grows due to the precipitation in the polar boxes, and decreases due to ablation, ice runoff, and calving processes.

2.2. Ocean Biogeochemistry Model

[14] Our biochemistry model is similar to those used in three-dimensional (3-D) biochemical general circulation models [e.g., *Bacastow and Maier-Reimer*, 1990; *Yamanaka*, 1996]. Its parameters appear in Table 2. The model includes total CO_2 (ΣCO_2) and alkalinity (A_T) (including the components of the aqueous carbon and borate only) as prognostic variables that are used to calculate pCO_2. PO_4 is taken to be the limiting nutrient in our model, as is commonly done in other model studies. This enables us to disregard the complex interaction between different components of the nitrogen cycle [*Maier-Reimer*, 1993]. The model is of the "closed-system" type [*Sigman and Boyle*, 2000], so total alkalinity and PO_4 are constant during the integration, although their distribution in the ocean can change. We also take into account the salinity and temperature calculated in the ocean model for calculation of the dissociation coefficients. Surface pCO_2 is calculated based on the ΣCO_2, alkalinity, salinity, and temperature and is computed according to *Yamanaka* [1996].

[15] The equations for ΣCO_2, A_T, and PO_4 are similar to those for the temperature and salinity, except for an added source/sink term S_p for the biochemistry variables,

$$P_t + (vP)_y + (wP)_z = K_h P_y + K_v P_z + S_p. \quad (3)$$

The source/sink is different for each variable, and the processes included in it are discussed below. Redfield ratio is the ratio between $P{:}N{:}C$ (assumed constant 1:16:122) in particulate organic matter. We denote the ratio $P{:}N$ as R_N and denote the ratio $P{:}C$ as R_C. The rate of export production, EP (the part of organic matter that is produced at the surface boxes and that sinks as particulate organic flux), depends on the latitude (via the light factor), the

Table 3. Experiments Summary

Experiment Code	Description	Figures
PHYSICS-ONLY	no ocean biochemistry effects, only physical components of the climate system	2
BIO	including ocean biochemistry	3
SIF	sea ice does not affect air-sea CO_2 flux	6
VM_M	oceanic vertical mixing in the midlatitude	7
VM_S1, VM_S2	oceanic vertical mixing in the south with and without insulating effect of sea ice	8
PV1,PV2	changes in the piston velocity	9
DM	deep horizontal mixing	10

amount of nutrients (PO_4 in our model), and the ocean area not covered by sea ice, $A_{openwater}$, and is given by

$$EP = rL_f[PO_4]A_{openwater}, \qquad (4)$$

where L_f is the light factor taken to be the averaged solar radiation at each box and $[PO_4]$ is the phosphate concentration; r serves as a tuning parameter, which enables us to take implicitly into account other factors that may affect the production, such as a lack of iron, and is therefore different for each box. A more realistic parameterization (similar to *Maier-Reimer* [1993]) is

$$EP = rL_f[PO_4]\frac{[PO_4]}{h + [PO_4]},$$

where h is a half-saturation constant and gives very similar results in our model because the relatively large thickness of the upper boxes in our model "smoothes" the variations in surface concentration found in GCMs that resolve the thermocline with a few levels. The sinking particles from each surface box are assumed to be remineralized in the deep box below. The specified "rain ratio" dictates the ratio of organic to inorganic carbon atoms extracted from the ΣCO_2 pool per PO_4 molecule that sinks as particulate flux. We use the same expression for the rain ratio (RR) as used by *Maier-Reimer* [1993]

$$RR = 61 \exp[0.1(T - 10)]/\{1 + \exp[0.1(T - 10)]\},$$

where T is the surface temperature. This expression gives an upper limit of 0.5 for the rain ratio.

[16] The source/sink terms for ΣCO_2, A_T (total alkalinity), and PO_4 are affected by numerous processes. We now consider the processes included in the source/sink term for each variable.

2.2.1. ΣCO_2

[17] Export production of organic soft tissue and of calcite shells reduces the ΣCO_2 at the surface at rates of $R_C \times EP$ and $RR \times EP$, respectively, and remineralization increases ΣCO_2 in the deep boxes at the same rates. Gas exchange of CO_2 between the atmosphere and the ocean also affects the ΣCO_2 content of the ocean. The flux between the ocean and the atmosphere is linear in the pCO_2 difference between atmosphere and the surface boxes of the ocean.

$$F_{CO_2} = PV([CO_{2,a}] - [CO_{2,o}])A_{openwater}, \qquad (5)$$

where $[CO_{2,a}]$ is the saturation concentration with regard to the partial pressure of CO_2 in the atmosphere, $[CO_{2,o}]$ is the concentration of CO_2 in the ocean, and $A_{openwater}$ is the ocean area not covered by sea ice, thus taking into account the influence of sea ice cover on the air-sea flux; PV is the piston velocity [*Siegenthaler and Sarmiento*, 1993]. Adding all these terms, we find, for a given surface box,

$$S_{\Sigma CO_2} = -R_C \times EP - RR \times EP + PV([CO_{2,a}] - [CO_{2,o}])$$

and for the deep box below it,

$$S_{\Sigma CO_2} = R_C \times EP + RR \times EP.$$

2.2.2. A_T (Total Alkalinity)

[18] The production of calcite shells at the surface reduces the alkalinity there at a rate of $2 \times RR \times EP$, and the dissolution of shells in the deep ocean increases the alkalinity at the same rate. The export production of soft tissue increases the alkalinity at the surface boxes at a rate of $R_N \times EP$, and remineralization in the deep boxes decreases it, again at the same rate. The source term for a surface box becomes

$$S_{A_T} = -2 \times RR \times EP + R_N \times EP,$$

while for a deep box, the signs of the terms are opposite.

2.2.3. PO_4

[19] Export production from the surface and remineralization in the deep ocean act as sink and source, respectively, for phosphate, at a rate of EP. Thus $S_{PO_4} = -EP$ at the surface and has the opposite sign in the box below.

3. Results

[20] All runs analyzed in this paper are summarized in Table 3. We begin by analyzing a physics-only model run (PHYSICS-ONLY) (Table 3) without the biochemistry ocean model and with a fixed atmospheric CO_2 (section 3.1). Having briefly discussed the sea ice switch mechanism of the glacial oscillations using this simplified run, we then add the ocean biochemistry model, which induces atmospheric CO_2 variability and therefore affects the atmospheric radiation balance (experiment BIO) (section 3.2). Then, sensitivity experiments are discussed in section 4. In order to test the effect of sea ice on the air-sea CO_2 flux [*Francois et al.*, 1997; *Stephens and Keeling*, 2000], we run experiment sea-ice-flux (SIF) (section 4.1), in which the existence of sea ice does not prevent CO_2 flux between

the ocean and the atmosphere, as it does in the full model and in the actual climate system. The influence of the vertical mixing between the midlatitude surface and deep boxes is investigated in experiment VM_M, and the sensitivity to a different vertical mixing parameterization between the surface and deep southern boxes is investigated in run VM_S (section 4.2). In runs PV1 and PV2 we check the sensitivity of the results to the piston velocity of air-sea CO$_2$ exchange (section 4.3). Finally, we investigate the sensitivity to the rate of deep horizontal mixing (experiment DM) (section 4.4).

3.1. Physics-Only Run

[21] The results of the physics-only run (without the ocean biogeochemistry and with a fixed atmospheric CO$_2$ using seasonal solar forcing based on present-day orbital parameters without Milankovitch variations) are shown in Figure 2. The oscillations are practically identical to those of *Gildor and Tziperman* [2000, 2001a] in spite of the few changed model details, but with a somewhat longer time-scale, as is discussed below. These glacial-interglacial oscillations result from a combination of the temperature-precipitation and temperature-albedo feedbacks [*Källén et al.*, 1979; *Ghil et al.*, 1987; *Ghil*, 1994]. However, both the timescale and the asymmetric sawtooth structure of the land ice volume time series (Figure 2a) are determined in our model by a novel sea ice feedback in which the sea ice grows and melts within a few decades and acts as a switch of the climate system, switching it between growing and retreating land ice modes. Briefly, the oscillation mechanism is as follows [*Gildor and Tziperman*, 2000, 2001a].

[22] Starting from an interglacial state, as the Northern Hemisphere land ice begins to grow from its minimum point (Figure 2a, year 170,000), the northern ocean is ice free (Figure 2b), and the atmospheric and oceanic temperatures in the northern box are rather mild (Figure 2f). The amount of precipitation enabling glacier growth exceeds the ablation, melting, and calving term (Figure 2e), and therefore the northern box glacier gradually grows. The resulting slow increase in land ice albedo slowly reduces the temperature of the atmosphere and of the ocean (Figure 2f) in the corresponding northern polar box. When the ocean sea surface temperature (Figure 2f) reaches the critical freezing temperature (around year 50,000), sea ice starts to form very rapidly (Figure 2b). The creation of sea ice further increases the albedo, induces a further reduction of atmospheric temperature, and results in the creation of more sea ice (positive feedback). In <20 years, ~60% of the polar box ocean surface is covered by sea ice. Sea ice stops growing when it isolates enough of the ocean from the cold atmosphere, reducing the air-sea cooling that leads to the sea ice formation. The sea ice switch is now turned to "on."

[23] At this stage, the average global temperature is at its lowest point, sea ice and land ice sheet extents are maximal, and the system is at a glacial maximum. Because of the low polar box atmospheric temperature, there is a large decline in poleward moisture flux, about half of its maximum value. Similarly, the sea ice cover limits the moisture extraction by evaporation from the polar ocean box and further reduces the corresponding snow accumulation over the land ice. As
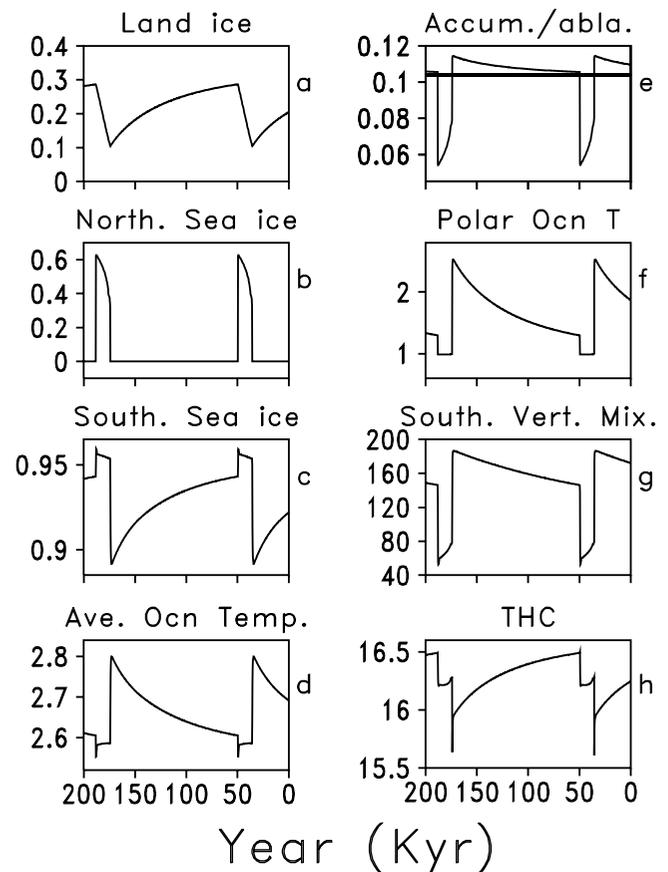
Figure 2. Physics-only run, with no ocean biochemistry and using fixed atmospheric CO$_2$. (a) Northern land ice extent as a fraction of polar land box area. (b) Northern sea ice extent as a fraction of polar ocean box area. (c) Southern sea ice extent as a fraction of polar ocean box area. (d) Oceanic averaged temperature (°C). (e) Source term (solid line) and sink term (dash line) for northern land glacier (10^6 m^3 s^{-1}). (f) Temperature in northern upper polar oceanic box (°C). (g) Vertical mixing between surface and deep southern boxes (10^6 m^3 s^{-1}). (h) Thermohaline circulation (THC) through northern polar boxes (10^6 m^3 s^{-1}).

ablation and glacier runoff proceed as before, being less sensitive to temperature than precipitation, the glaciers start retreating. The land albedo decreases again, and the atmospheric temperature rises slowly. This is the beginning of the termination stage of the glacial period. The upper ocean in the polar box is at freezing temperature as long as sea ice is present. However, once the deep ocean warms enough to allow the upper ocean to warm as well, the sea ice melts within ~40 years. (Similar rapid retreat of sea ice may have occurred at the end of the Younger Dryas [*Dansgaard et al.*, 1989]). The sea ice switch is now turned to "off," the temperature of both the atmosphere and the ocean are at their maximum values, and the system is at an interglacial state, having completed a full glacial cycle.

[24] One important improvement in the present results over the results of *Gildor and Tziperman* [2000, 2001a] is the new glacial-interglacial variability of the Southern

Ocean and of the Southern Ocean sea ice cover, resulting from the improved parameterizations described in section 2.1 (Figure 2c). While Southern Ocean sea ice exists throughout the model glacial cycle, its meridional extension now varies between glacial and interglacial states, as well as varying with the seasonal cycle, and depends on the conditions in the Northern Hemisphere. When sea ice is present in our model's northern polar box, the deep water that is formed there and that fills the deep ocean becomes colder. This causes two effects that contribute to the increased extension of southern sea ice: (1) The temperature of the upwelling water in the Southern Ocean is colder, and (2) the vertical stratification in the Southern Ocean becomes more stable; hence less vertical mixing occurs between the surface and deep southern polar boxes. The significant effect of the upwelling water on the evolution of sea ice in the Southern Ocean is known from both observational and model studies [*Martinson*, 1990; *Gordon*, 1981; *Gordon and Huber*, 1990]. The reduced vertical mixing will be further discussed in section 3.2 and section 4.2 and will be seen later to play an important role in the glacial-interglacial CO$_2$ cycle, when the biogeochemistry is activated, as expected from work by *Toggweiler* [1999]. In turn, it will be shown that the CO$_2$ cycle intensifies the glacial-interglacial cycle of the Southern Ocean sea ice extent. Unlike in the work by *Toggweiler* [1999], the vertical mixing and the THC in our model are not specified, but are calculated by the model equations and vary during the glacial-interglacial cycles. Consistent with observations, the THC through our northern box weakens during cold glacial periods [*Boyle and Keigwin*, 1987].

3.2. Biogeochemistry Effects

[25] Figure 3 shows the model results obtained when activating the ocean biogeochemistry, its effects on the atmospheric CO$_2$, and the radiative effects of a variable CO$_2$. Note that all model parameters used in this section are the same as those in run PHYSICS-ONLY of section 3.1 and that the atmospheric concentration of CO$_2$ in the PHYSICS-ONLY run is fixed at the lowest value of CO$_2$ concentration seen in the variable CO$_2$ experiment here, specifically, 200 ppm. While the glacial-interglacial cycle in the physical climate system is qualitatively unchanged, as can be seen from the northern land ice extension time series (Figure 3a), some important changes do occur, including a reduction of the timescale to 100 kyr. First, there is a difference of ~75 ppm in atmospheric CO$_2$ between glacial and interglacial periods. Atmospheric CO$_2$ concentration is highest at the beginning of an interglacial period, after the sea ice cover in the north vanishes (sea ice switch turned to off) and the sea ice cover in the south reaches its minimal extension (year 165,000 in Figure 3b). The atmospheric CO$_2$ concentration then decreases gradually as the land ice grows and the ocean cools, reaching its minimum just before the northern sea ice melts. As in the four-box model of *Toggweiler* [1999], the Southern Ocean in our model is a source of CO$_2$ to the atmosphere, while the northern box serves as a sink.

[26] The glacial-interglacial variations in atmospheric CO$_2$ may be explained as the result of a competition between the upwelling of deep nutrient-rich water in the Southern Ocean and the vertical mixing of this deep water with surface water
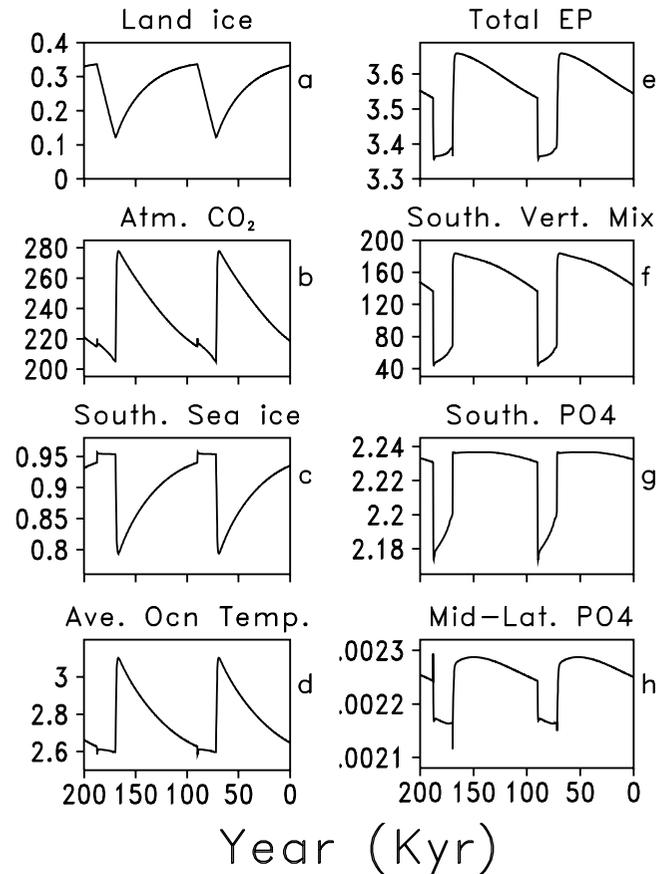
Figure 3. Run BIO with active biochemistry. (a) Northern land ice extent as a fraction of polar land box area. (b) Atmospheric concentration of CO$_2$ (ppm). (c) Southern sea ice extent as a fraction of polar ocean box area. (d) Oceanic averaged temperature (°C). (e) Total export production (Gt C yr^{-1}). (f) Vertical mixing between surface and deep southern boxes (10^6 m^3 s^{-1}). (g) PO$_4$ concentration in southern surface box (μmol, kg); (h) PO$_4$ concentration in midlatitude surface box (μmol, kg).

of the Southern Ocean, as follows [*Toggweiler*, 1999]. The upwelling of deep water in the Southern Ocean by the THC brings to the surface nutrients as well as CO$_2$-rich water; these nutrients are then advected northward to midlatitudes, where they are utilized for biological production [*Toggweiler*, 1999], which results in a flux of particulate carbon to the deep ocean. The particulate flux of carbon dominates the upwelling of carbon in the form of CO$_2$-rich water, resulting in a reduction of the surface pCO$_2$. Conversely, vertical mixing in the Southern Ocean brings to the surface water rich with CO$_2$, which can escape to the atmosphere, leaving nutrient-rich water in the surface Southern Ocean. The biological pump in the Southern Ocean is not efficient, due to the lack of light and micronutrients (such as iron), so that the net effect of the vertical mixing in the Southern Ocean is to increase the surface pCO$_2$ there. Thus the relative strength of vertical mixing in the Southern Ocean compared to the upwelling and meridional advection by THC dictates the atmospheric concentration of CO$_2$. The
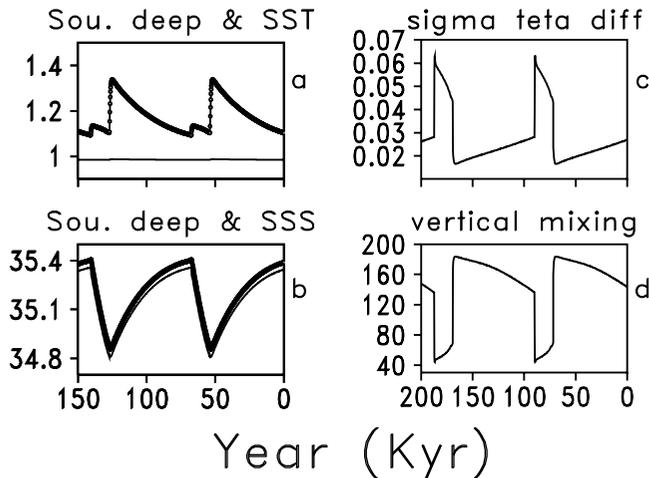
Figure 4. Vertical structure of water column in the Southern Ocean. (a) Ocean temperature (°C) of surface (thin line) and deep (thick line) boxes. (b) Ocean salinity of surface (thin line) and deep (thick line) boxes. (c) Difference of σ_θ between deep and surface boxes (kg). (d) Vertical mixing between surface and deep southern boxes (10^6 m³ s⁻¹).

reduced rate of vertical mixing during glacial times allows less CO_2 from the deep water to escape into the atmosphere and results in a reduced atmospheric CO_2.

[27] The vertical mixing changes in the Southern Ocean that play such a critical role were specified by *Toggweiler* [1999]. Yet here they turn out to be a natural consequence of the sea ice switch mechanism, due to changes to the vertical stratification in the Southern Ocean, through the mixing parameterization of *Gargett* [1984], as specified in equation (1). As can be seen in Figures 4a and 4b, while the salinities of the southern deep and surface boxes vary together during the glacial-interglacial cycle, their temperatures do not. Because Antarctica is always covered by ice, even during interglacial periods, the temperature of the adjacent water cannot rise by much, and sea ice is present in the southern surface box during the entire glacial-interglacial cycle. Therefore the sea surface temperature (SST) in the southern box stays at the critical temperature of 1° (the "freezing" temperature in our model). Conversely, the temperature of the deep box changes as the temperature of NADW becomes colder because of the ice sheet expansion. The NADW temperature signal is then transferred to the deep and Southern Ocean and affects the stratification there. Because the vertical mixing depends on the water column stratification through equation (1), we expect a higher rate of vertical mixing during warm interglacial periods. This is precisely the change of mixing needed, as specified by *Toggweiler* [1999], without a physical mechanism, which we can provide here.

[28] The total export production out of the three surface boxes ranges from 3.35 to 3.65 Gt C yr⁻¹ (Figure 3e), seemingly on the lower side of existing estimates [*Siegenthaler and Sarmiento*, 1993]. Note, though, that the depth of our surface boxes is 400 m, well below the euphotic zone. Taking into account that up to 90% of the export production is remineralized above 400 m [*Suess*, 1980], our

implied results for export production from the euphotic region are actually somewhat above the current estimates. We have made this choice while building the model for the following reason. The vertical gradient in biochemical properties within the upper 400 m is quite significant, with much of the vertical gradient limited to the euphotic region. Representing this profile with a single value, as is done in this model, results in an obvious bias and hence in possibly unrealistic results for the pCO₂, for example. There are two ways to deal with this problem. The first, which is employed here, is to artificially increase the export production to the deep water below 400 m depth. Another possibility is to specify as surface values of pCO₂, for example, some fraction of the box average and to use this adjusted surface value for the air-sea flux calculation. We have tried both procedures and found them to result in similar model solutions.

[29] During the glacial-interglacial cycles the southern box acts as a source of atmospheric CO_2, having pCO₂ up to 100 ppm higher than the atmosphere during glacial maxima. The northern polar box acts as a sink, with pCO₂ up to 50 ppm lower than that of the atmosphere. The oceanic midlatitude box pCO₂ is slightly above (up to 2 ppm) that of the atmosphere, but because of its large area it also acts as a significant source of atmospheric CO_2 in our model.

[30] One important issue that has not been studied so far and that our present model allows us to examine is the mutual feedbacks between the physical and biochemical components of the climate system. We begin by comparing the Northern Hemisphere ice sheet cycles with and without the biochemistry model (Figure 5a).

[31] In run BIO the size of the ice sheet (Figure 5a, thin line) needed to switch on the sea ice cover is larger than in the PHYSICS-ONLY run. Conversely, in order to turn the sea ice switch to off, only slightly more land ice needs to melt in run PHYSICS-ONLY. The reason for these differences is clear from the sensitivity experiments done by *Gildor and Tziperman* [2001a]: The atmospheric CO_2 is allowed to change and to affect the radiation balance in run BIO. As atmospheric CO_2 is lower in the PHYSICS-ONLY run during the buildup stage of land ice sheets (Figure 5b), the climate system cools faster than in the BIO run. Hence a smaller land ice sheet extent is needed in order to cool the ocean and form a sea ice cover. The atmospheric CO_2 changes amplify the ice-albedo effect, as expected from the high correlation found between CO_2 and an atmospheric temperature proxy in the Vostok ice core [*Petit et al.*, 1999] and from other model results [*Weaver et al.*, 1998]. During the deglaciation, atmospheric CO_2 is approximately equal in the two runs; therefore the land ice needs to melt down to about the same size to sufficiently warm the atmosphere and the ocean in order to melt the sea ice. After the sea ice melts and the climate enters an interglacial period, atmospheric CO_2 rises, and the climate is warmer compared to the PHYSICS-ONLY run. Because of the temperature-precipitation feedback the land ice sheet grows more quickly (Figure 5a).

[32] The amplification of the glacial-interglacial cycle by the ocean biochemistry through its effects on the atmospheric CO_2 concentration can be seen in many other model variables. Figures 5c and 5d, for example, present a sig-
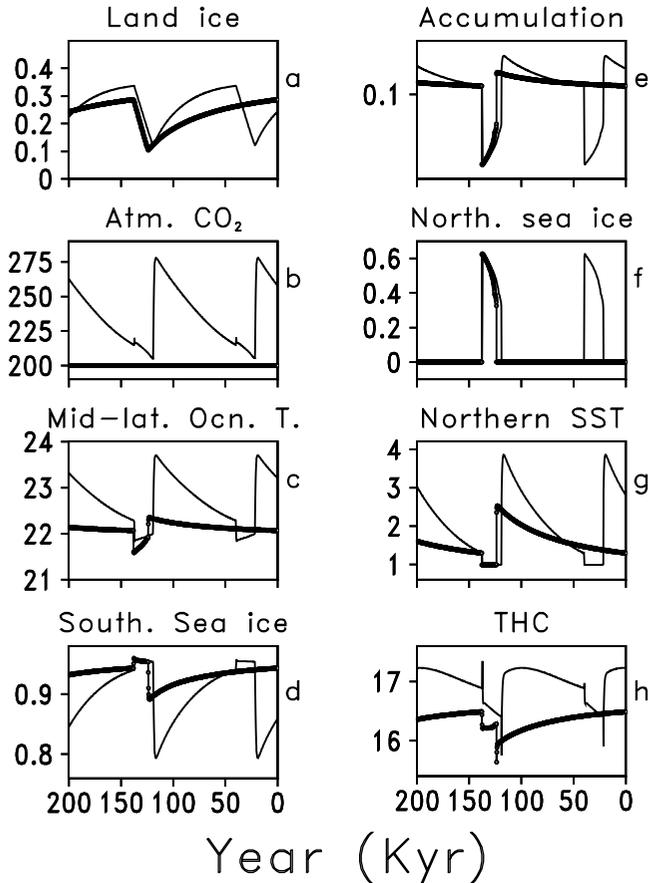
Figure 5. Comparison between PHYSICS-ONLY (thick lines) and BIO (thin lines) experiments. (a) Northern land ice extent as a fraction of polar land box area. (b) Atmospheric concentration of CO_2 (ppm). (c) Midlatitude oceanic temperature (°C). (d) Southern sea ice extent as a fraction of polar ocean box area. (e) Source term for northern land glacier (10^6 m^3 s^{-1}). (f) Northern sea ice extent as a fraction of polar ocean box area. (g) Temperature in northern upper polar oceanic box (°C). (h) THC through northern polar boxes (10^6 m^3 s^{-1}).

nificant amplification of the glacial-interglacial signal in the annual mean oceanic temperature in the midlatitude box and in the sea ice extent in the Southern Ocean. The variations during the glacial-interglacial cycles are consistently larger in run BIO than in run PHYSICS-ONLY. The correlation between the Southern Ocean sea ice extent and atmospheric CO_2 may explain the high correlation found between the CO_2 and atmospheric temperature proxy in the Vostok ice core [*Petit et al.*, 1999]. While in our model the atmospheric concentration of CO_2 is not the driving force of the glacial-interglacial oscillation, there is clearly a two-way feedback between the physical components of the climate system and the ocean biochemistry: The stratification changes induced by the glacial-interglacial cycle cause variations in atmospheric CO_2, which, in turn, amplify the glacial-interglacial cycle in the physical components of the climate system.

[33] The observed relative phasing between changes in atmospheric CO_2, land ice volume, and oceanic and atmos-

pheric temperature is still being debated, and currently available proxies cannot rule out the assumption, implied in our mechanism, that the Northern Hemisphere leads the south [*Gildor and Tziperman*, 2001b, and references therein]. About 2000 years pass in our model from the time of sea ice melting in the Northern Hemisphere to the time of maximum atmospheric CO_2, minimum extension of Southern Ocean sea ice, and temperature changes in the Southern Hemisphere. The rapid changes in northern ocean surface temperature resulting from the fast retreat of the sea ice immediately affect the pCO_2 of the surface ocean, and hence affect the atmospheric CO_2. While this change in CO_2 also affects the Southern Hemisphere atmospheric temperature and sea ice extension, it takes a longer time for the full signal transported by the NADW temperature to reach the Southern Ocean, and only then does the Southern Ocean sea ice reach its minimal extent (hence its minimal albedo) and the atmospheric CO_2 reach its maximal concentration.

4. Sensitivity Tests

[34] The differences between box models and GCMs were the focus of numerous recent works [*Archer et al.*, 2000a; *Broecker et al.*, 1999]. Understanding these differences and assessing the ability of both box models and GCMs to simulate correctly the carbon cycle is crucial, not only in order to test different mechanisms for the glacial-interglacial CO_2 variations, but also to improve our ability to simulate oceanic uptake of anthropogenic CO_2, in which different GCMs differ substantially from each other [*Orr et al.*, 2001].

[35] An extensive series of sensitivity tests for key parameters of the physical model has been conducted and described by *Gildor and Tziperman* [2001a]. The mechanism and timescale of the 100-kyr oscillation were shown to be quite robust, and we therefore do not repeat these sensitivity experiments here. The sensitivity of ocean biochemistry models to parameters such as the rain ratio and the Redfield ratio has also been examined in previous studies [*Heinze et al.*, 1991]. Therefore we wish to concentrate here on a brief discussion of the sensitivity to a few processes that have recently been debated in the literature in the context of box models versus GCMs. These are the insulating effect of a Southern Ocean sea ice cover (section 4.1), the vertical mixing between the deep and surface ocean (section 4.2), the piston velocity (section 4.3), and the horizontal mixing in the deep ocean (section 4.4). T01a and T01b addressed the box model versus GCM issue in some detail. They argue that differences in air-sea partitioning due to solubility effects and organic cycling need to be examined separately. They concluded that box models with northern and southern sources of deep water, such as *Toggweiler*'s [1999], *Stephens and Keeling*'s [2000], and the model employed in the current study, represent the air-sea partitioning of CO_2 due to organic cycling more accurately than do GCMs.

4.1. Effects of Southern Ocean Sea Ice Cover on Atmospheric CO₂ Variability

[36] Southern Ocean sea ice cover changes have been proposed recently to be responsible for a major part of the drawing down of atmospheric CO_2 during glacial times
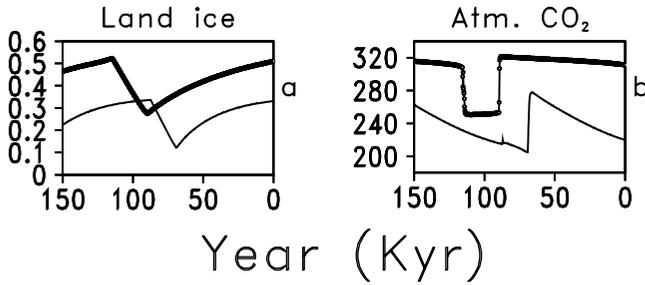
Figure 6. Comparison between BIO (thin line) and SIF (thick line) experiments showing deactivated sea ice cover insulating effect on air-sea CO$_2$ flux. (a) Northern land ice extent as a fraction of polar land box area. (b) Atmospheric concentration of CO$_2$ (ppm).

[*Francois et al.*, 1997; *Stephens and Keeling*, 2000]. Sea ice cover has an insulating effect on air-sea CO$_2$ flux, and this effect is included in our model. We tried to evaluate the effects of changes in sea ice cover on glacial-interglacial atmospheric CO$_2$ variability by removing its insulating influence on air-sea fluxes from the model (run SIF).

[37] The difference in atmospheric CO$_2$ concentration between glacial and interglacial is quite similar in the two runs (Figure 6b), amounting to ~75 ppm. The structure of the glacial-interglacial CO$_2$ cycle, however, is very different between the two runs, pointing to the possible role of the sea ice cover in shaping the structure of the CO$_2$ cycle. The glacial-interglacial difference in CO$_2$ in both the control run and run SIF is due to the change in the Southern Ocean vertical mixing, as discussed in section 3.2. When the sea ice cover affects the air-sea flux (control run), the slow evolution of the Southern Ocean sea ice also induces a slow drawdown of atmospheric CO$_2$. Without the insulating effects of Southern Ocean sea ice, the CO$_2$ changes abruptly, jumping between two states, approximately following the change in vertical mixing. (In addition, note that the CO$_2$ concentration is higher overall when we remove the sea ice cover effect on air-sea CO$_2$ flux (Figure 6b).)

[38] Our time-dependent model also seems to indicate that an extensive sea ice cover variability alone may not be able to explain the difference between glacial and interglacial atmospheric concentration of CO$_2$. In an experiment (not shown) in which we assign a fixed rate of vertical mixing between the surface and deep southern boxes, there was a very weak glacial-interglacial difference in atmospheric CO$_2$ concentration, regardless of the sea ice cover insulating effect on the air-sea flux. In another experiment in which the vertical mixing parameterization is modified so that vertical mixing changes more gradually between glacial and interglacial periods (section 4.2), the atmospheric CO$_2$ changes gradually as well, even without including the sea ice insulating effect.

[39] Given the simplicity of our box model, it is clearly impossible to evaluate the quantitative importance of the sea ice cover in shaping the oscillation structure. The southern sea ice cover in our model is too large, during both glacial and interglacial periods, and it may therefore bias the evaluation of the sea ice role. Also, the uncertainties in

the value of the piston velocity (section 4.3) and the demonstrated sensitivity to this parameter [*Broecker et al.*, 1999] are relevant to this issue: We show in section 4.3 that when the piston velocity is sufficiently large, the influence of glacial-interglacial variations in Southern Ocean sea ice cover on atmospheric CO$_2$ becomes significantly smaller.

4.2. Oceanic Vertical Mixing

[40] In experiment BIO the vertical mixing between the deep and surface midlatitude boxes was set to a constant rate of 0.5 Sv, while that between the northern surface and deep boxes was 5 Sv. Recently, *Bacastow* [1996], *Archer et al.* [2000a, 2000b], and *Broecker et al.* [1999] have suggested that the sensitivity of box models to high-latitude processes might be the result of an absent or too low rate of vertical mixing between the depth and surface of the midlatitude ocean. In experiment VM_M (VERTICAL-MIXING MID-LATITUDE) we double the vertical mixing rate between the surface and deep midlatitude boxes. Note that besides the vertical mixing between the surface and deep midlatitude boxes, there is also a unidirectional upwelling from the midlatitude deep box, usually missing in other box models, such as those of *Toggweiler* [1999] and *Stephens and Keeling* [2000]. Additional vertical mixing is expected to add nutrients to the upper surface box, enabling enhanced productivity and hence reduced pCO$_2$. Conversely, the stronger mixing also brings CO$_2$-rich water to the surface, where, because of the relatively high temperature at midlatitudes, part of the CO$_2$ degasses into the atmosphere. At the warm midlatitudes the degassing effect may dominate the enhanced productivity, leading to an increased atmospheric CO$_2$ [*Pedersen and Bertrand*, 2000]. In our model the glacial-interglacial variations in atmospheric CO$_2$ are somewhat smaller when the vertical mixing is stronger (thick line in Figure 7) than in experiment BIO [*Archer et al.*, 2000a]. The role of vertical mixing parameters and parameterizations clearly needs to be examined further.

[41] The model sensitivity to the mixing parameterization in the Southern Ocean (equation (1)) is examined in runs VM_S1 and VM_S2. We add $\Delta\sigma$ to the denominator of equation (1), making it

$$K_v^0 \left(\sigma_{t_{\text{deep}}} - \sigma_{t_{\text{surface}}} + \Delta\sigma \right)^{-\alpha} \left(Tr_{\text{deep}} - Tr_{\text{surface}} \right), \tag{6}$$

where $\Delta\sigma = 0.02$. The physical motivation for adding the $\Delta\sigma$ factor is that in our box model the entire area of the
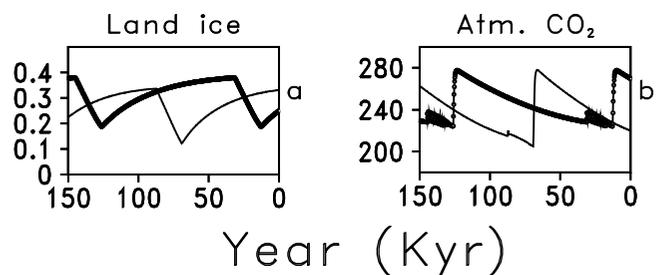
Figure 7. Comparison between BIO (thin line) and VM_M (thick line) experiments. (a) Northern land ice extent as a fraction of polar land box area. (b) Atmospheric concentration of CO$_2$ (ppm).
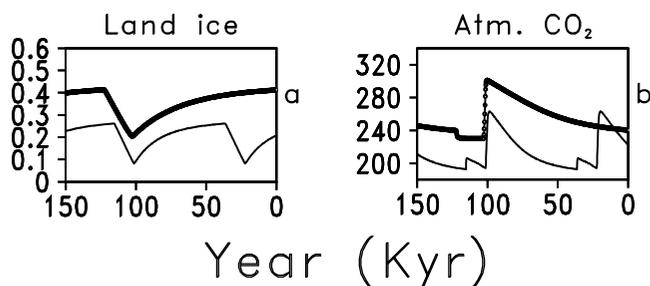
Figure 8. Results obtained with a different vertical mixing parameterization between southern box (VM_S) with (thin line) and without (thick line) sea ice effect on air-sea flux. (a) Northern land ice extent as a fraction of polar land box area. (b) Atmospheric concentration of CO_2 (ppm).

Southern Ocean is represented by a single value of the density, so that it is either all convecting or all stably stratified. In reality, it is possible that while some regions would be convecting, others would not. The above parameterization causes the changes in the rate of vertical mixing to be more gradual as a function of the density difference between the upper and lower levels, roughly representing a gradually increasing area of convection as the vertical density difference becomes smaller. We use this somewhat artificial representation because we want to examine the consequences on the atmospheric CO_2 of a gradual increase in mixing along the glacial cycle, as opposed to the two-state mixing behavior of Figures 4d and 6. Using equation (3), we have run the coupled model with (experiment VM_S1) and without (experiment VM_S2) the insulating sea ice effect. The thin line in Figure 8 shows the results obtained when sea ice cover affects the air-sea CO_2 flux, while the thick line is as in run SIF; that is, sea ice cover does not affect air-sea CO_2 flux. We can see that as before, the existence of sea ice cover causes a general drawdown of ~40 ppm. But unlike in SIF, the CO_2 decline during the buildup stage of the ice sheet is gradual, following the gradual changes of the vertical mixing between the surface and deep southern boxes.

[42] These sensitivity experiments indicate that the the CO_2 reduction during glacial times in our model is the result of a reduced ventilation by mixing in the Southern Ocean, with the sea ice playing a relatively minor role. This conclusion may clearly be very model dependent, and we cannot rule out the possibility that sea ice does play a more significant role in controlling atmospheric CO_2 in the actual climate system.

4.3. Piston Velocity

[43] There is a large uncertainty in the parameters governing the air-sea flux of CO_2 between the ocean and the atmosphere, up to a factor of 2 between different estimates for the piston velocity appearing in equation (5) [*Siegenthaler and Sarmiento*, 1993]. The piston velocity is highly dependent on the winds [*Bates and Merlivat*, 2001], an effect neglected in simple box models (which might have been amplified during glacial periods). The high sensitivity of model results to the piston velocity was

recently discussed by *Broecker et al.* [1999], but this high sensitivity was suggested to be partly due to the lack of vertical mixing between the surface and deep midlatitude water. The lack of this mixing means that the atmosphere is the major factor connecting the warm water with the cold deep water masses when they outcrop in polar areas. It is interesting, therefore, to examine the sensitivity to the piston velocity in our model, which does contain such vertical mixing and which also simulates the evolution along the glacial-interglacial cycle, rather than treating the glacial and interglacial as two steady states.

[44] To look into this issue, we double (run PV1) and cut by half (run PV2) the value of the piston velocity, and the results can be seen in Figure 9. The difference between the amplitudes of atmospheric CO_2 variability in the two runs amounts to ~45 ppm, with an accompanying difference in the amplitude of the land ice sheet cycle. The model is clearly quite sensitive to the rate of air-sea CO_2 exchange, confirming previous results using simpler box models.

[45] Interestingly, most of the difference comes from the reduced piston velocity experiment. The model is more sensitive to variations in this parameter when its value is low than when it is large. T01a and T01b investigated further the role played by gas exchange, which is affected by both the piston velocity and the effective outcrop area, and attributed to it the difference between box models and GCMs. They separated the effect of gas exchange on the solubility and on organic pumps. T01a deals with the solubility pump and show that, indeed, doubling the piston velocity or increasing the outcrop area when the initial outcrop area is large have negligible effect. In contrast, the response grows exponentially when the outcrop area is small. T01a concludes that the effective area for gas exchange in the real world probably lies somewhere between box models and GCMs. The mechanism behind the glacial-interglacial CO_2 variations in our model, however, is not driven by the solubility pump (as confirmed by an experiment in which the dissociation coefficients were independent of temperature changes, not shown). When taking into consideration the organic pump as well, T01b shows that box models that divide the "generic" high-latitude box used in classical three-box models [*Sarmiento and Toggweiler*, 1984; *Volk and Hoffert*, 1985] into southern and northern boxes (like *Toggweiler*'s [1999], *Stephens and*
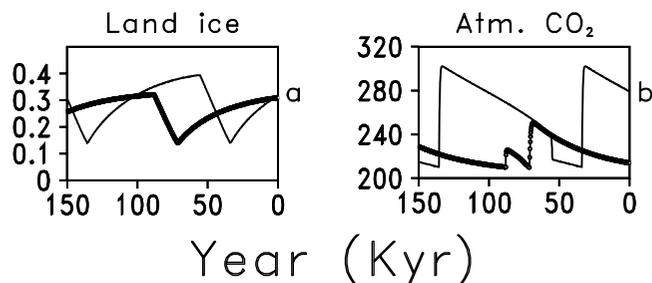
Figure 9. Model results for runs PV for increasing (thin line) and decreasing (thick line) piston velocity. (a) Northern land ice extent as a fraction of polar land box area. (b) Atmospheric concentration of CO_2 (ppm).
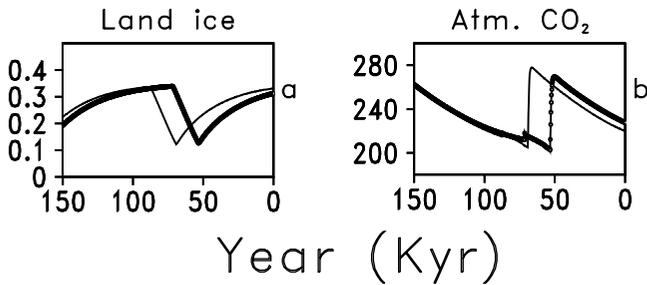
Figure 10. Comparison between BIO (thin line) and DM (thick line) experiments. (a) Northern land ice extent as a fraction of polar land box area. (b) Atmospheric concentration of CO_2 (ppm).

Keeling's [2000], and the model used in this study) seem to do better than GCMs. Certainly, the sensitivity to the piston velocity and the effective area for gas exchange should be further examined.

4.4. Horizontal Mixing in the Deep Ocean

[46] Simple box models usually treat the deep ocean as a single box [*Volk and Hoffert*, 1985; *Wenk and Siegenthaler*, 1985; *Stephens and Keeling*, 2000]. Our model, with three meridional deep boxes, thus represents a slight improvement in resolution. Nevertheless, it is important to note that a relatively high rate of horizontal mixing between the deep boxes was necessary in order to get satisfactory results for glacial-interglacial CO_2 changes ($K_{h_{deep}}$ is $\sim$120 Sv, which is some 20 times larger than it was in the physics-only runs of *Gildor and Tziperman* [2000, 2001a]. The results of a run using half the value of $K_{h_{deep}}$ are presented in Figure 10. The amplitude of the glacial-interglacial CO_2 is almost 10 ppm less than in the BIO experiment. Even this halved mixing rate is still relatively high, and the fact that the we were forced to use such a large and unrealistic value of horizontal deep mixing may indicate that there is a problem with the mechanism used here to explain the glacial-interglacial CO_2 variability. This problem did not arise in previous studies [*Volk and Hoffert*, 1985; *Wenk and Siegenthaler*, 1985; *Stephens and Keeling*, 2000] because they were using a single well-mixed deep box. This issue needs to be further examined using still higher resolution models that resolve the deep circulation, which accounts for some of the deep horizontal mixing crudely parameterized in box models.

5. Conclusions

[47] We have investigated the role of ocean biochemistry in the glacial-interglacial cycles and the interaction between the physical and biochemical components of the climate system using a time-dependent coupled physical-biochemical model. Previous studies indicated that a change to the vertical mixing [*Toggweiler*, 1999] and sea ice changes [*Stephens and Keeling*, 2000] in the Southern Ocean may account for the glacial-interglacial CO_2 variability, without indicating what might be the cause of such changes. Our results here suggest a specific novel physical mechanism by which vertical mixing in the Southern Ocean may have

changed during the glacial-interglacial cycles, as follows. The glaciation in the Northern Hemisphere induces a gradual cooling there, which also cools the deep water formed in the North Atlantic. This colder deep water temperature is transported southward by the thermohaline circulation and affects the stratification in the Southern Ocean, which is composed of cold fresh water above the warmer but saltier water mass influenced by the North Atlantic Deep Water (NADW). The flow of colder NADW from the north cools the subsurface water but not the surface water in the Southern Ocean, which is already near the freezing point and cannot cool further. This makes the water column there during cold periods more stable, thus reducing vertical mixing between the surface and deep waters of the Southern Ocean. These vertical mixing changes, in turn, contribute, in our model, $\sim$75 ppm to the reduction of atmospheric CO_2 during glacial periods, based on the mechanism of *Toggweiler* [1999].

[48] The changes in vertical mixing and in the temperature of the NADW reaching the Southern Ocean also explain the extended sea ice cover in the Southern Ocean during cold glacial periods that is strongly affected by the temperature of the upwelling deep water and explain the synchronous climate change between the two hemispheres. These vertical mixing and sea ice cover changes, required to explain the glacial CO_2 variations, were shown here to be a natural result of the sea ice switch mechanism for the glacial cycle suggested by *Gildor and Tziperman* [2000, 2001a].

[49] While the changes in the physical state of the ocean during the glacial-interglacial cycles induce changes in the atmospheric concentration of CO_2, the resulting effect on the atmospheric radiation balance, in turn, amplifies the glacial cycle in the physical climate system. Thus, while the CO_2 changes are not the driving force behind the glacial-interglacial oscillation in our model [*Loutre and Berger*, 2000], they do contribute to the amplitude of the cycles, as expected from the recent Vostok analysis [*Petit et al.*, 1999].

[50] The scenario for CO_2 changes presented by *Gildor and Tziperman* [2001b] and presented here predicts that the warming of the Southern Ocean and the phase of maximum atmospheric CO_2 concentration may have occurred after the Northern Hemisphere warming and the onset of the deglaciation. Presently available proxy data cannot yet resolve the phasing between these events. In any case, our model provides a self-consistent description of the 100-kyr cycle, the interhemispheric teleconnection, and the CO_2 cycle that may possibly be verified or falsified with the future availability of more accurate proxy records, in particular, records of sea ice cover [*de Vernal*, 1997; *de Vernal and Hillaire-Marcel*, 2000; *de Vernal and Pedersen*, 1997; *Gersonde and Zielinski*, 2000].

[51] The purpose of the present model being highly idealized is to qualitatively explore possible mechanisms that may have played a role in glacial-interglacial dynamics. As isotopic signatures (e.g., $\delta^{13}C$ and $\delta^{15}N$) seem to be highly dependent on the fine structure details of the meridional circulation in simplified box models (compare, e.g., the differences between the four- and seven-box cases of *Toggweiler* [1999]), we did not try to reconstruct isotopic proxies from our model results. Sensitivity experiments

demonstrate that our results are generally robust, but further investigation is required, especially regarding the role of piston velocity and deep horizontal mixing. Recent works (T01a and T01b) confirmed that there is a strong sensitivity to gas exchange and polar area. Despite our model's limitations, we feel that the results are at least plausible and can explain some of the main aspects of both the physical and biochemical glacial oscillations.

[52] Other processes not included in our model, such as alkalinity changes, have certainly contributed to the observed atmospheric CO$_2$ cycles. We have used a constant Redfield ratio, although recent observations in the Southern Ocean show that depending on the local stratification, different phytoplankton species with different Redfield ratios may dominate [*Arrigo et al.*, 1999]. The resulting changes in the Redfield ratio can be >50%, with the higher C/P ratio species being dominant in less stratified water [*Arrigo et al.*, 1999]. Our model predicts a more stable stratification in the Southern Ocean during glacial maximum but a less stably stratified ocean in the midlatitudes, as the surface ocean there has cooled more than the deep ocean. Additional contribution to the drawdown of atmospheric CO$_2$ during glacial times might have arisen, had the Redfield ratio at midlatitudes changed during the glacial cycles due to these midlatitude stratification changes based on a similar mechanism as observed in higher latitudes by *Arrigo et al.* [1999]. Our main result is the possible physical mechanism resulting in vertical mixing and sea ice cover changes in the Southern Ocean, and it would be most interesting to see this mechanism examined using fuller general circulation models and new proxy data.

References

Archer, D., G. Eshel, A. Winguth, W. Broecker, R. Pierrehumbert, M. Tobis, and R. Jacob, Atmospheric pCO$_2$ sensitivity to the biological pump in the ocean, *Global Biogeochem. Cycles*, 14, 1219–1230, 2000a.

Archer, D., A. Winguth, D. Lea, and N. Mahowald, What caused the glacial/interglacial atmospheric pCO$_2$ cycles?, *Rev. Geophys.*, 38, 159–189, 2000b.

Arrigo, K. R., D. H. Robinson, D. L. Worthen, R. B. Dunbar, G. R. DiTullio, M. VanWoert, and M. P. Lizotte, Phytoplankton community structure and the drawdown of nutrients and CO$_2$ in the Southern Ocean, *Science*, 283, 365–367, 1999.

Bacastow, R., The effect of temperature change of the warm surface waters of the ocean on atmospheric CO$_2$, *Global Biogeochem. Cycles*, 10, 319–333, 1996.

Bacastow, R., and E. Maier-Reimer, Ocean circulation model of the carbon cycle, *Clim. Dyn.*, 4, 95–125, 1990.

Bates, N., and L. Merlivat, The influence of short-term wind variability on air-sea CO$_2$ exchange, *Geophys. Res. Lett.*, 28, 3281–3284, 2001.

Boyle, E. A., and L. Keigwin, North Atlantic thermohaline circulation during the past 20,000 years linked to high-latitude surface temperature, *Nature*, 330, 35–40, 1987.

Broecker, W., J. Lynch-Stieglitz, D. Archer, M. Hofmann, E. Maier-Reimer, O. Marchal, T. Stocker, and N. Gruber, How strong is the Harvadton-Bear constraint?, *Global Biogeochem. Cycles*, 13, 817–820, 1999.

Crosta, X., J. Pichon, and L. Burckle, Application of modern analog technique to marine Antarctic diatoms: Reconstruction of maximum sea ice extent at the Last Glacial Maximum, *Paleoceanography*, 13, 284–297, 1998.

Dansgaard, W., J. White, and S. Johnsen, The abrupt termination of the Younger Dryas climate event, *Nature*, 339, 532–534, 1989.

Daskal Hausman, E., and M. B. McElroy, Role of sea surface temperature and ocean circulation changes in the reorganization of the global carbon cycle at the last glacial termination, *Global Biogeochem. Cycles*, 13, 371–381, 1999.

de Vernal, A., Sea-surface conditions in the northwest North Atlantic during the Last Glacial Maximum, *GEOTOP contrib. 97-001*, Cent. for Res. in Isotopic Geochem. and Geochronol., Univ. of Quebec, Montreal, Que., Canada, 1997. (Available at http://www.unites.uqam.ca/geotop/18ka.html)

de Vernal, A., and C. Hillaire-Marcel, Sea-ice cover, sea-surface salinity and halo/thermo-cline structure of the northwest North Atlantic: Modern versus full glacial condition, *Quater. Res.*, 19, 65–85, 2000.

de Vernal, A., and T. F. Pedersen, Micropaleontology and palynology of core par87a-10: A 23,000 year record of paleoenvironmental changes in the Gulf of Alaska, northeast North Pacific, *Paleoceanography*, 12, 821–830, 1997.

Francois, R., M. A. Altabet, E. Yu, D. M. Sigman, M. P. Bacon, M. Frank, G. Bohrmann, G. Bareille, and L. D. Labeyrie, Contribution of Southern Ocean surface-water stratification to low atmospheric CO$_2$ concentrations during the last glacial period, *Nature*, 389, 929–935, 1997.

Ganopolski, S., A. Rahmstorf, V. Petoukhov, and M. Claussen, Simulation of modern and glacial climates with a coupled global model of intermediate complexity, *Nature*, 391, 351–356, 1998.

Gargett, A., Vertical eddy diffusivity in the ocean interior, *J. Mar. Res.*, 42, 359–393, 1984.

Gersonde, R., and U. Zielinski, The reconstruction of late quaternary Antarctic sea-ice distribution: The use of diatoms as a proxy for sea-ice, *Paleogeogr. Paleoclimatol. Paleoecol.*, 162, 263–286, 2000.

Ghil, M., Cryothermodynamics: The chaotic dynamics of paleoclimate, *Physica D*, 77, 130–159, 1994.

Ghil, M., A. Mulhaupt, and P. Pestiaux, Deep water formations and Quaternary glaciations, *Clim. Dyn.*, 2, 1–10, 1987.

Gildor, H., and E. Tziperman, Sea ice as the glacial cycles climate switch: Role of seasonal and Milankovitch solar forcing, *Paleoceanography*, 15, 605–615, 2000.

Gildor, H., and E. Tziperman, A sea ice climate switch mechanism for the 100-kyr glacial cycles, *J. Geophys. Res.*, 106, 9117–9133, 2001a.

Gildor, H., and E. Tziperman, Physical mechanisms behind biogeochemical glacial-interglacial CO$_2$ variations, *Geophys. Res. Lett.*, 28, 2421–2424, 2001b.

Gnanadesikan, A., A simple predictive model for the structure of the oceanic pycnocline, *Science*, 283, 2077–2079, 1999.

Gordon, A., Seasonality of Southern Ocean sea ice, *J. Geophys. Res.*, 86, 4193–4197, 1981.

Gordon, A., and B. Huber, Southern Ocean winter mixed layer, *J. Geophys. Res.*, 95, 11,655–11,672, 1990.

Heinze, C., E. Maier-Reimer, and K. Winn, Glacial pCO$_2$ reduction by the world ocean: Experiments with the Hamburg carbon model, *Paleoceanography*, 4, 395–430, 1991.

Källén, E., C. Crafoord, and M. Ghil, Free oscillations in a climate model with ice-sheet dynamics, *J. Atmos. Sci.*, 36, 2292–2303, 1979.

Loutre, M., and A. Berger, No glacial-interglacial cycle in the ice volume simulated under a constant astronomical forcing and a variable CO$_2$, *Geophys. Res. Lett.*, 27, 783–786, 2000.

Maier-Reimer, E., Geochemical cycles in an ocean general circulation model: Preindustrial tracer distribution, *Global Biogeochem. Cycles*, 7, 645–677, 1993.

Martinson, D., Evolution of the Southern Ocean winter mixed layer and sea ice: Open ocean deepwater formation and ventilation, *J. Geophys. Res.*, 95, 11,641–11,654, 1990.

Matsumoto, K., and J. Lynch-Stieglitz, Similar glacial and holocene deep water circulation inferred from southeast Pacific benthic foraminiferal carbon isotope composition, *Paleoceanography*, 14, 149–163, 1999.

Maykut, G., and D. Perovich, The role of shortwave radiation in summer decay of a sea ice cover, *J. Geophys. Res.*, 92, 7032–7044, 1987.

Orr, J., et al., Estimates of anthropogenic carbon uptake from four three-dimensional global ocean models, *Global Biogeochem. Cycles*, 15, 43–60, 2001.

Pedersen, T., and P. Bertrand, Influence of oceanic rheostats and amplifiers on atmospheric CO$_2$ content during the late Quaternary, *Quat. Sci. Rev.*, 19, 273–283, 2000.

Petit, J. R., et al., Climate and atmospheric history of the past 420,000 years from the Vostok ice core, Antarctica, *Nature*, 399, 429–436, 1999.

Ramanathan, V., et al., Climate-chemical interaction and effects of changing atmospheric trace gases, *Rev. Geophys.*, 25, 1441–1482, 1987.

Sarmiento, J. L., and J. R. Toggweiler, A new model for the role of the oceans in determining atmospheric pCO$_2$, *Nature*, 308, 621–624, 1984.

Schrag, D., G. Hampt, and D. Murray, Pore fluid constraints on the tem-

perature and oxygen isotopic composition of the glacial ocean, *Science*, *272*, 1930–1932, 1996.

Siegenthaler, U., and J. Sarmiento, Atmospheric carbon dioxide and the ocean, *Nature*, *365*, 119–125, 1993.

Sigman, D. M., and E. A. Boyle, Glacial/interglacial variations in atmospheric carbon dioxide, *Nature*, *407*, 859–869, 2000.

Sikes, E. L., C. R. Samson, T. P. Guilderson, and W. R. Howard, Old radiocarbon ages in the southwest Pacific Ocean during the last glacial period and deglaciation, *Nature*, *405*, 555–559, 2000.

Stephens, B. B., and R. Keeling, The influence of Antarctic sea ice on glacial-interglacial CO$_2$ variations, *Nature*, *404*, 171–174, 2000.

Stommel, H., Thermohaline convection with two stable regimes of flow, *Tellus*, *13*, 224–230, 1961.

Suess, E., Particulate organic carbon flux in the oceans: Surface and oxygen utilization, *Nature*, *288*, 260–262, 1980.

Toggweiler, J. R., Variation of atmospheric CO$_2$ by ventilation of the ocean's deepest water, *Paleoceanography*, *14*, 572–588, 1999.

Toggweiler, J. R., and B. Samuels, Is the magnitude of the deep outflow from the Atlantic Ocean actually governed by the Southern Hemisphere winds?, in *The Global Carbon Cycle, NATO ASI Ser. 1*, vol. 15, edited by M. Heimann, pp. 303–331, Springer-Verlag, New York, 1993.

U.N. Educational, Scientific, and Cultural Organization, Tenth report of the Joint Panel on Oceanographic Tables and Standards, *Tech. Rep.*, *36*, Paris, 1981.

Volk, T., and M. Hoffert, Ocean carbon pumps: Analysis of relative strengths and efficiencies in ocean-driven atmospheric CO$_2$ changes, in *The Carbon Cycle and Atmospheric CO$_2$: Natural Variations Archean to Present, Geophys. Monogr. Ser.*, vol. 32, edited by E. T. Sundquist and W. S. Broecker, pp. 99–110, AGU, Washington, D. C., 1985.

Weaver, A. J., M. Eby, A. Fanning, and E. C. Wiebe, Simulated influence of carbon dioxide, orbital forcing and ice sheets on the climate of the Last Glacial Maximum, *Nature*, *394*, 847–853, 1998.

Weertman, J., Milankovitch solar radiation variations and ice age ice sheet sizes, *Nature*, *261*, 17–20, 1976.

Wenk, T., and U. Siegenthaler, The high-latitude ocean as a control of atmospheric CO$_2$, in *The Carbon Cycle and Atmospheric CO$_2$: Natural Variations Archean to Present, Geophys. Monogr. Ser.*, vol. 32, edited by E. T. Sundquist and W. S. Broecker, pp. 185–194, AGU, Washington, D. C., 1985.

Yamanaka, Y., Development of ocean biogeochemical general circulation model, *Tech. Rep. 1*, Cent. for Clim. Sys. Res., Univ. of Tokyo, Tokyo, 1996.

Yu, E.-F., R. Francois, and M. P. Bacon, Similar rates of modern and last-glacial ocean thermohaline circulation inferred from radio-chemical data, *Nature*, *379*, 689–694, 1996.

————————————

H. Gildor and E. Tziperman, Environmental Sciences, Weizmann Institute of Science, Rehovot 76100, Israel. (hezi.gildor@weizmann.ac.il; eli@beach.weizmann.ac.il)

J. R. Toggweiler, Geophysical Fluid Dynamics Laboratory, National Oceanic and Atmospheric Administration, P.O. Box 308, Princeton, NJ 08542, USA. (jrt@gfdl.noaa.gov)

Figure 1. Schematic representation of coupled box model used in this study, showing atmospheric boxes (upper slab), thermohaline circulation (arrows), parabolic land ice sheets over land, and a partial sea ice cover in the polar ocean boxes. All of these physical climate system components are allowed to vary based on model equations. Ocean biogeochemistry and atmospheric CO_2 fully interact with physical climate components.